Intercomparison of SCIAMACHY and SIM vis-IR irradiance over several solar rotational timescales

J. Pagaran[1], J. W. Harder[2], M. Weber[1], L. E. Floyd[3], and J. P. Burrows[1]

[1] Institute of Environmental Physics (IUP), Department of Physics and Engineering, University of Bremen, Otto-Hahn-Allee 1, 28359 Bremen, Germany
e-mail: pagaran@iup.physik.uni-bremen.de
[2] Laboratory for Atmospheric and Space Physics (LASP), University of Colorado, 1234 Innovation Drive, Boulder, CO 80303, USA
[3] Interferometrics Inc., 13454 Sunrise Valley Drive, Herndon, Virginia, VA 20171, USA

ABSTRACT

The two satellite spectrometers SCIAMACHY (SCanning Imaging Absorption spectroMeter for Atmospheric CHartographY) aboard ENVISAT (Environmental Satellite), and SIM (Spectral Irradiance Monitor) aboard SORCE (Solar Radiation and Climate Experiment) observe since 2002 and 2003, respectively, daily solar spectral irradiance (SSI) not only in UV but extending to the visible and near- infrared (vis-NIR) regions. In this work, we intercompare (1) spectra and (2) timeseries of SSI measurements from SCIAMACHY and SIM. In (1) same-day (April 21, 2004) SSI measurements from these two instruments are compared to reference spectra from ground (new Kurucz), high-altitude (Hall and Anderson, Neckel and Labs, and Wehrli composite), and space (SOLSPEC/ATLAS 3, and SUSIM/UARS). In (2) timeseries of measurements (July 3 to August 21, 2004) covering several solar rotations in 2004 are compared to VIRGO sunphotometers (SPM) aboard SOHO. In general, SCIAMACHY and SIM are in agreement to within 4% over the common spectral domain and with respect to the other reference data. Apart from SSI and its variability, we integrate SSI over selected wavelength intervals and compare qualitatively to total solar irradiance (TSI) variability from PMOD/WRC and TIM/SORCE. Timeseries of integrated SSI in the vis (400–700 nm), NIR (700–1600 nm), and UV-vis-NIR (240–1600 nm) bands are compared. The overall rise and fall of integrated SCIAMACHY and SIM irradiances over several solar rotations are in good agreement and agree in most cases qualitatively with TSI variations in the visible and near IR. The application of White Light Source (WLS) corrections brings SCIAMACHY irradiances in closer agreement with SIM. Since WLS is also degrading with time, the WLS lamp ratios cannot be used for SSI degradation corrections after 2004.

Key words. Sun: activity – Sun: faculae, plages – Sun: infrared – Sun: photosphere – Sun: rotation – sunspots

1. Introduction

The variability of solar irradiance is a strong function of wavelength. The knowledge on how it varies as a function of wavelength is a key in understanding solar-stellar (Hudson 1988; Berdyugina 2005; Nandy & Martens 2007; Hall 2008; Priest 2009), and solar-terrestrial connections (Hoyt & Schatten 1997; Lean 1997; Lean & Rind 2001; Arnold 2002; Fröhlich & Lean 2004; Haigh 2003, 2007; Rind et al. 2008; Domingo et al. 2009; de Wit & Watermann 2010; Gray et al. 2010). Our present understanding of solar spectral irradiance (SSI) variability is based on direct SSI measurements in the UV (Lean 1987; Woods & Rottman 2002; Rottman et al. 2004) and visible-infrared (vis-IR) regions (Harder et al. 2005a,b; Pagaran et al. 2009). Regular daily UV measurements from space began in the late 1970s, while vis-IR measurements just started in the 2000s with the launch of SCIAMACHY and SIM (see Fig. 1). According to the Intergovernmental Panel on Climate Change (IPCC) Report (2001), the level of scientific understanding (LOSU) on UV solar irradiance variations is medium to high while the LOSU of vis-NIR variations are poor, since there were only model estimates available by then. Since the launch of SCIAMACHY aboard ENVISAT (2002-present) (Bovensmann et al. 1999; Skupin et al. 2005a,b; Gottwald et al. 2006) and SIM aboard SORCE (2003-present) (Harder et al. 2000, 2005a,b), first quantitative statements on the variability of solar output in the visible and

near-IR could be made. See for example, Fontenla et al. (2004); Unruh et al. (2008); Harder et al. (2009); Pagaran et al. (2009). Despite the limited time coverage of these direct SSI measurements, they provide the starting point for reconstructing SSI in the pre-satellite, telescopic and even pre-telescopic era (Lean et al. 1997; Tobiska et al. 2000; Lean et al. 2005; Krivova et al. 2006; Tobiska & Bouwer 2006; Pagaran et al. 2009; Krivova et al. 2009, 2011) these SSI reconstructions are nevertheless used, for example, as "realistic" solar input to general circulation models (GCMs) in assessing the overall role of the changing sun in a changing terrestrial climate (Haigh 2003, 2007; de Wit & Watermann 2010).

SSI variability is the spectral decomposition of "solar constant" or total solar irradiance (TSI) variability. The contribution to TSI is roughly 70% from the vis-IR spectral region and less than 30% from UV. During an 11-year solar cycle, TSI varies by 0.1% between solar maximum and minimum or during a 27-day solar rotation by up to 0.2–0.3% depending on the level of sunspot activity (Fröhlich & Lean 2004; Rottman 2006). About half of TSI variability comes from the UV, i.e., about 30–60% (Lean et al. 1997; Krivova et al. 2006; Pagaran et al. 2009), the remainder from vis-IR. However, not all spectral regions vary in the same phase with TSI as shown by SCIAMACHY (Pagaran et al. 2009) and SIM (Harder et al. 2009) observations. Even though the radiometric calibration in SCIAMACHY, primarily an earth atmosphere sounder, has a somewhat lower priority than
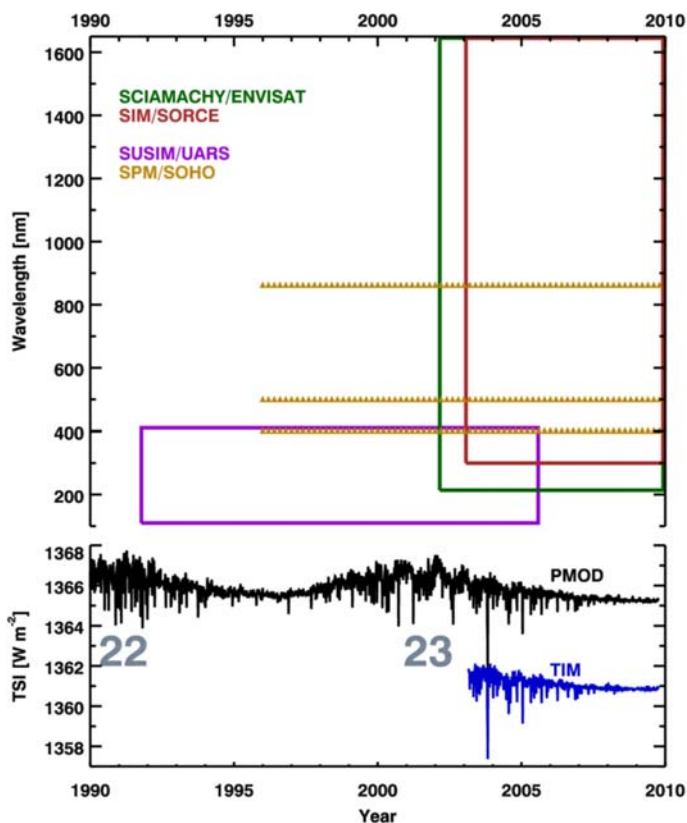
Fig. 1. SSI and TSI measurements as used in this study. Top sub-panel shows wavelength ranges and time coverage of SSI measurements from SUSIM/UARS (purple), VIRGO SPM/SOHO (tan), SCIAMACHY/ENVISAT (green), and SIM/SORCE (maroon). Bottom subpanel shows TSI from PMOD/WRC composite (black) and TIM/SORCE (blue) measurements.

for dedicated solar satellite spectrometry like SIM, its stability is sufficient to detect changes, e.g., at the per-mill level in vis-IR, over brief periods like 27-day solar rotation (Pagaran et al. 2009). As an advanced version of GOME (Burrows et al. 1999; Weber et al. 1998) aboard ERS-2, SCIAMACHY is a multi-channel grating spectrometer, whose primary aim is the retrieval of trace gases in the Earth's atmosphere on a global scale. The employment of multiple gratings is to resolve spectral absorption features from scattered sunlight (upwelling radiance) by the Earth's atmosphere. The ratio of the upwelling radiance and SSI, which is inverted to provide information about the amounts and distribution of important atmospheric constituents, does not require to first order absolutely calibrated SSI. In contrast, as an extension and replacement to SOLSTICE (Rottman et al. 1993; Rottman & Woods 1994) aboard UARS, SIM is a single-element spectrometer, whose primary aim is to measure spectral irradiance, i.e., at a sufficient precision and accuracy, thereby producing a reliable record of short and multi-year solar variations (Rottman 2005; Harder et al. 2009).

Below, we discuss two aspects of comparison: (1) the shape of the solar spectra (spectral aspect) and (2) the vis-NIR variations over several solar rotations (time aspect). In the past years, comparisons focusing on (1) consider most of the available reference spectra including SIM. They have been made, for example, in Gueymard (2004, 2006) but without taking into account the spectral response function (slit function) of the individual instruments. In contrast, proper use of instrument function were made in comparisons between SIM and SRPM

spectral synthesis (Fontenla et al. 2004; Harder et al. 2005c; Fontenla & Harder 2005); SCIAMACHY and SIM to several reference spectra (Gurlit et al. 2005; Skupin et al. 2005a,b; Piters et al. 2006). Most recent comparison using SCIAMACHY has been made by Dobber et al. (2008) but it was limited to the 250–550 nm wavelength range. Recently in Harder et al. (2010), SIM has been compared to Thuillier et al. (2004) reference spectrum. Comparisons focusing on (2) were restricted to the three color channels of the SPM instrument of SOHO/VIRGO (Fligge et al. 1998, 2000; Unruh et al. 2008); this restriction is observed in the present work. In Unruh et al. (2008), SATIRE semi-empirical model was compared to SIM across the UV-vis-IR spectrum as well as over 27-day solar rotational time scales. We extend their work by adding SCIAMACHY to SIM comparisons and by using other time periods (from July 3 to August 21, 2004). During this time interval, significant solar activity occurred (Harder et al. 2005c) thereby significantly increasing signal-to-noise ratio (S/N) especially in vis-NIR regions. Detecting NIR variations reaches the instrumental noise levels during quiet Sun periods. Most of these studies did not investigate how the changes of SSI and integrated changes of SSI over selected wavelength intervals compare to changes of TSI over several rotational time scales. We will pursue the latter comparisons but only qualitatively.

With the new archive of solar data from SCIAMACHY and SIM starting in 2002 and 2003, respectively; and the various intercomparisons made in the past few years, there is a need to validate SSI measurements from SCIAMACHY and SIM with emphasis on the vis-NIR regions. This will be done in this work as follows. Section 2 describes the reference and time-series solar data used in the validation. Section 3 intercompares SCIAMACHY and SIM irradiances as a function of wavelength and time, and SCIAMACHY and SIM integrated irradiances over selected wavelength intervals. Finally, Sect. 4 presents the discussion and conclusion of this study. An Appendix is included to provide a short overview on the instrumentation and in-flight calibration mechanisms of the two radiometers.

2. Data

In this section, first we give a brief overview of the two spectrometers: SCIAMACHY and SIM. Then we briefly describe the SSI data that are used for intercomparison.

2.1. SCIAMACHY and SIM instruments

The overview provides a short description on the design of these two instruments. Refer to Appendix A for additional information about the instruments.

SCIAMACHY aboard ENVISAT, 240–2380 nm, 2002-present. SCIAMACHY is a passive remote sensing imaging double spectrometer, which is a combination of a predispersing prism and gratings. Detailed description of SCIAMACHY can be found in Bovensmann et al. (1999); Gottwald et al. (2006); Pagaran et al. (2009).

Before the light enters the spectrometer, it passes through a scanner module (elevation and/or azimuth scanner) and a telescope (off-axis parabolic mirror) before reaching the entrance slit. The light is then collimated and directed onto the predispersing prism. This prism also serves as a Brewster window to separate polarized light, which is recorded at low spectral resolution using polarization monitoring devices (PMD).
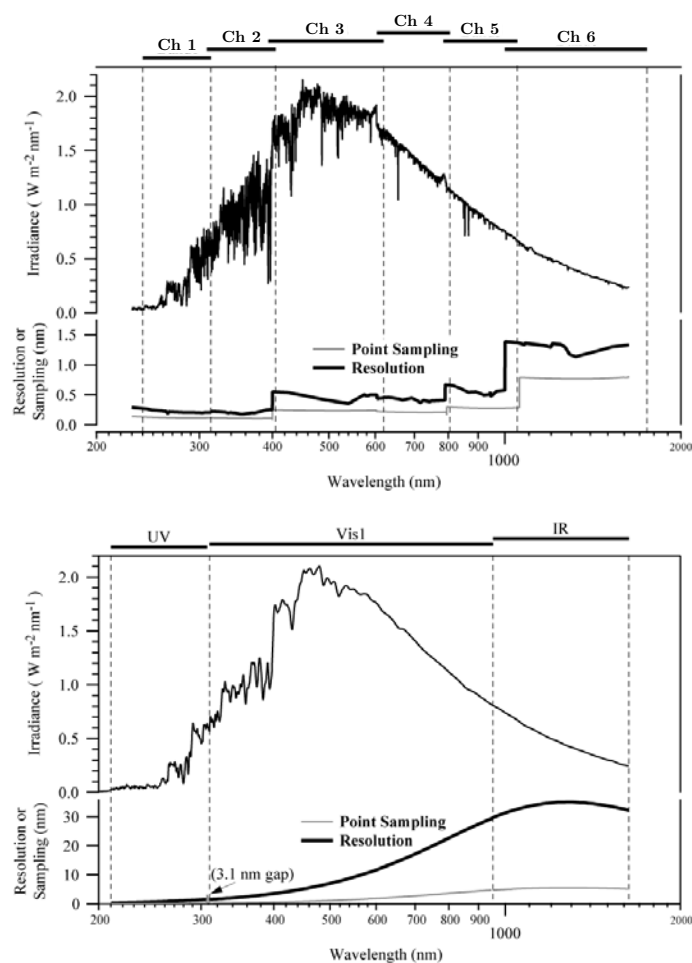
Fig. 2. Sample UV/vis-NIR solar spectra from SCIAMACHY (*top*) and SIM (*bottom*). Both spectra are taken on April 21, 2004. Listed in each panel are channels (SCIAMACHY) or spectral (SIM) bands, point sampling and spectral resolution. Boundaries between channels or bands are indicated by vertical dashed lines.

The prism separates the light into eight different channels. Reflected parts of the spectrum at shorter and longer wavelengths are directed to Channels 1–2 and 7–8, respectively. Unreflected parts of the spectrum are directed to Channels 3–6, where separate dichroic mirrors are employed to select wavelength ranges for each channel. An additional dichroic mirror is used to separate light further into SWIR spectral components in Channels 7 and 8.

Each channel has its own grating, transmission optics, and diode array detector. The role of the grating is to disperse the light into a high resolution part of the spectrum before the light is directed onto a linear 1024 pixel detector array. Silicon monolithic Reticon RL 1024 SR diode arrays developed by EG&G and InGaAs detectors by Epitaxx, Inc are used in Channels 1–5 and Channels 6–8, respectively.

SCIAMACHY has three optical paths for measuring solar irradiance, namely: calibration, limb, and nadir optical paths. These paths pass through ASM (azimuth scan mirror) mirror and ESM (elevation scan mirror) diffuser, ASM and ESM mirrors (limb), and ESM mirror only (nadir), respectively. Only the combination of ESM and ASM mirrors has been radiometrically calibrated before launch using FEL lamps.

A sample SCIAMACHY spectrum measured on April 21, 2004 is shown in Fig. 2 (top panel). For this and daily spectra,

we use version 6.03 SCIAMACHY data. For optical degradation corrections, particularly in the UV bands, the internal white lamp source (WLS), a quartz-halogen tungsten lamp, can be used to track changes with time in the optical throughput. The WLS corrections are described in Appendix A. In this study both SCIAMACHY data without degradation correction and with WLS corrections are compared. Since the WLS light path also suffers from optical degradation, the WLS corrections are not recommended for SCIAMACHY data after 2004.

SIM aboard SORCE, 300–2400 nm, 2003-present. SIM is a dual Fèry prism spectrometer that employs only one optical element to focus and disperse the light into parts of spectrum. It is a dual spectrometer consisting of two mirror image spectrometers; one for daily measurements while the other is used on a monthly basis to perform degradation corrections; SIM B has about 22% of the exposure rate of SIM A. Comprehensive account of the SIM design and operation can be found in Harder et al. (2005a,b, 2010).

Light from the entrance slit is directed to the prism, which rotates on a flex pivot with a flex suspended voice coil motor. The light is separated and directed to the exit slit, where an electrical substitution radiometer (ESR) and four photodiodes (UV, vis1, vis2, and NIR) simultaneously measure spectral irradiance at four neighboring wavelength ranges. In total, five independent detectors with overlapping wavelength coverage are used.

Every three months, an entire UV/vis-NIR scan is recorded with the ESR, which is the primary detector, but weekly ESR measurements are performed at selected wavelengths for the degradation corrections. The four photodiodes, which is a combination of Si and InGaAs diodes, provide two daily scans in the 200 to 1629 nm range. Two of these are the vis1 and vis2 photodiodes, which are constructed similarly but with *n*-on-*p* and *p*-on-*n* geometries, respectively. Due to increased levels of detector degradation due to proton bombardment, scan from the vis2 diode is not reported. For wavelength calibration purposes, a separate optical path passing to a steering mirror then onto a CCD is described in Appendix A.

A sample SIM[1] spectrum measured on April 21, 2004 is shown in Fig. 2 (bottom panel). For this and daily spectra, we use version 13 SIM data.

2.2. Solar data used for intercomparison

In the intercomparison, we are interested in two aspects: (1) spectral, and (2) time aspects. While the first aspect considers irradiance data as a function of wavelength, the second aspect considers irradiance data not only as a function of wavelength but also as a function of time.

In addition to intercomparing SCIAMACHY and SIM comparisons between the two and the following SSI data are made: (1) ground-based (2) high-altitude (rockets, balloon, or aircraft), and (3) other space-borne measurements. These spectra and the types of comparison considered are summarized in Table 1.

Ground-based measurements. New Kurucz spectrum[2] is an extremely high resolution spectrum (e.g., 0.0005 nm) from 300 to 1000 nm. It is based on re-reduced McMath-Pierce Fourier Transform Spectrometer (FTS) scans from Kitt Peak National

---

[1] http://lasp.colorado.edu/sorce/data/ssi_data.htm
[2] See, for example, in
http://kurucz.harvard.edu/sun/IRRADIANCE2005/

Table 1. Solar spectra used in this study for comparisons.

Spectral intercomparison			
Ground-based & high-altitude	Wavelength range [nm]	Resolution [nm] /Increment[nm]	References
Hall and Anderson	200–310	~0.025/0.01	Hall & Anderson (1991)
Neckel and Labs	330–1250	2/1 to 5	Neckel & Labs (1984)
New Kurucz or Kitt Peak	300–1000	<0.005 /0.0003 to 0.001	Kurucz (1995)
Wehrli composite	200 to 10 000	0.4–2/1 to 2	Wehrli (1985)
Space-borne spectra	Wavelength range [nm]	Resolution [nm] /Increment[nm]	References
SOLSPEC/ATLAS 3 composite	200–2400	1/0.015 to 1	Thuillier et al. (2004)
SUSIM/UARS	120–410	0.15/0.05	Brueckner et al. (1993, 1995)
Timeseries intercomparison			
Selected SSI data	Wavelength range [nm]	Time period	References
RGB from VIRGO/SPM	402, 500, and 862	1996-present	Fröhlich et al. (1995)
Selected TSI data	average TSI	Time period	References
PMOD/WRC	1367 W m^{-2}	1978-present	Fröhlich & Lean (1998)
TIM/SORCE	1361 W m^{-2}	2003-present	Kopp et al. (2005)

Solar Observatory that made up the Kitt Peak Solar Flux Atlas by Kurucz (1995).

High-altitude measurement. The Hall and Anderson reference spectrum (Hall & Anderson 1984; Anderson & Hall 1989; Hall & Anderson 1991) are composed from balloon measurements near 40 km in April of years 1977–78, 1980–81, and 1983. It is a composite spectrum composed of 1983 data from 200.00–207.74 nm and normalized 1978 data from 207.75–310.00 nm. It has a sampling rate of 0.01 nm that has been obtained by block averaging over 5 samples in the original data for purposes of data manageability. No significant artefacts have been found as a result of this block averaging.

The Neckel and Labs spectrum (Labs & Neckel 1968; Neckel & Labs 1981, 1984) spectrum is a three-band UV/vis-IR composite. It is composed of rocket data (200–330 nm), scaled HAO radiance data (330–1250 nm), and various other sources (above 1250 nm). The latter spectral regions were observed in the early 1960's at the Jungfraujoch Scientific Station (Neckel & Labs 1984). Their last revision (Neckel & Labs 1984) took into account measured center-to-limb variation obtained from the Kitt-Peak National Solar Observatory using the Jungfraujoch instrument.

The PMOD/WRC composite from Wehrli (1985) was developed as a UV/vis-NIR composite from existing datasets, which were concatenated to cover most of the spectrum (200 nm–10 μm); the datasets are obtained from various sources: Neckel & Labs (1981), aircraft, rocket, and balloon data. The resulting composite spectrum is constrained such that its integrated irradiance is equal to the WMO-recommended solar constant value of 1367 W m^{-2}. This constraint is applied on the assumption that the irradiance below 199 nm and above 10 μm are negligible.

Space-borne measurements. The SOLSPEC/ATLAS-3 composite is based on irradiance measurements performed during the ATLAS missions on board the Space Shuttle (Thuillier et al. 2004; Harder et al. 2010). These missions are Spacelab (1982), ATLAS 1-2-3 flights (1992–1994), and the SOlar SPectrum (SOSP) on EURECA mission (1993–1994). The composite has a wavelength range from 200–2400 nm. SSI in 200–400 nm is from SSBUV, SUSIM and SOLSPEC data (ATLAS mission) and SOLSTICE and SUSIM data (UARS). SSI in 400–800 nm is from SOLSPEC data, above 800 nm from SOSP NIR data. Its spectral resolution is 0.25 nm (sampling rate of 0.05 nm) in 200–400 nm and 0.5 nm above 400 nm (variable sampling of 0.2 to 0.6 nm).

SUSIM aboard UARS is a dual dispersion spectrometer, which consists of two independent double-monochromators (Brueckner et al. 1993, 1995). For comparison, we use version 22 SUSIM[3] spectrum (mid-resolution) that was measured on April 21, 2004 through scanning mode (Floyd et al. 2003).

The VIRGO/SOHO sunphotometers (SPM) are filter radiometers that measure solar variability in three wavelength bands: 402 (Blue), 500 (Green) and 862 nm (Red) with bandwidths ($FWHM$) of 5.4, 5.0 and 5.7 nm, respectively (Wehrli & Fröhlich 1991; Fröhlich et al. 1995). The profiles of the bandpass filters are shown in Fig. 8 in Sect. 3 below. We use version 20 level 2.0 hourly data that have been obtained from the SOHO data archive[4].

Produced as early as 1997, TSI composite from PMOD/WRC was the first to be constructed from different TSI measurements (Fröhlich & Lean 1998). In our comparison below, we use the composite d41 61 0810 version[5]. For the time period in summer 2004 considered in this study the TSI data in the PMOD/WRC composite stem from VIRGO (Fröhlich et al. 1995; Fröhlich 2003).

At a much higher relative precision and absolute accuracy, TIM aboard SORCE instrument is a new generation TSI radiometer, a state-of-the-art electrical substitution radiometer (Kopp et al. 2005). It measures TSI to an estimated absolute accuracy of 350 ppm (0.035%) and TSI relative changes up to less than 10 ppm/yr (0.001%/yr). The TSI values from TIM

---

[3] http://wwwsolar.nrl.navy.mil/susim_uars_data.html
[4] SPM data are available from ftp://ftp.pmodwrc.ch/pub/data/ irradiance/virgo/SSI/SPM_lev20a_h_170496_290508.dat; see also ftp://ftp.pmodwrc.ch/pub/Claus/SORCE_Sep2006/ SSI_Poster.pdf
[5] See, for example, ftp://ftp.pmodwrc.ch/pub/data/irradiance/composite/ DataPlots/composite_d41_61_0810.dat

are consistently 4–5 W m^{-2} less than TSI from other data, i.e., 1361 W m^{-2}. This issue has yet to be resolved. Daily SORCE TSI values are available from 2003 up to present. In our analysis we use the version 9 TSI data[6].

Among the irradiance data sets, the first seven and last three irradiance data sets (SPM VIRGO, PMOD and TIM TSI) are used in spectral and timeseries intercomparisons, respectively.

3. Intercomparison of UV/vis and NIR Solar Measurements

In this section intercomparisons are made by taking into full consideration the instrument profiles or slit function of the individual SSI measurements. In a given set of SSI data to be compared, spectra of relatively high spectral resolution are convolved to the SSI measurement that has the least spectral resolution. The convolution is done using the best known slit function of the instrument. When the slit function is not known, all wavelengths are rebinned to that of the spectrum having the least spectral resolution, thereby putting all spectra on a common wavelength scale; this is performed before we calculate integrated flux over a wavelength range.

In our comparison, SSI values are expressed by ratio with respect to a reference spectrum.

3.1. SSI comparison: same-day solar spectra

First, we compare SSI measurements from SCIAMACHY and SIM that are measured on a particular day to reference spectra. In general, the reference spectra are obtained from different dates or composite of them. The discrepancies are too small (in order of parts per mill) to be significant.

Together with the instrument's profile, spectral coverage, and spectral resolution, Fig. 2 shows SCIAMACHY and SIM spectra that were measured on April 21, 2004, along with plots of spectral resolution and point sampling as a function of wavelength. Shown are a SCIAMACHY spectrum without WLS correction and a SIM spectrum with bias correction as described in Harder et al. (2010). The latter is the standard SIM data product that is publicly available.

In this figure, only the wavelength range of up to 1600 nm is shown since the spectral channels 7 and 8 suffer from strong contamination (see also Fig. A.3). For subsequent analysis, we use triangular instrument line shapes for convolving reference data. SIM covers about six elements per resolution element while SCIAMACHY is close the to the Nyquist frequency limit of two data points per resolution elements for most parts of the spectrum. The *FWHM* of the SCIAMACHY line shape has been determined of emission lines of the Pt/Ne/Cr/Ar lamp (SLS). The SIM instrument line shape is determined from realistic ray trace analysis of the instrument and then verifying the profile area matches the result of the instrument scans done with laser sources. The trapezoidal shape of the instrument profile is ray traced for about 100 wavelengths over each detectors operating range. The trapezoidal profile can be determined for any wavelength by interpolation.

Wavelength uncertainty can be responsible for significant uncertainty in UV irradiance (Woods et al. 1996), which can become the dominant source of uncertainty towards the short wavelengths. Figure 3 shows a plot of absolute UV irradiances at 200–320 nm from SIM, SCIAMACHY, and
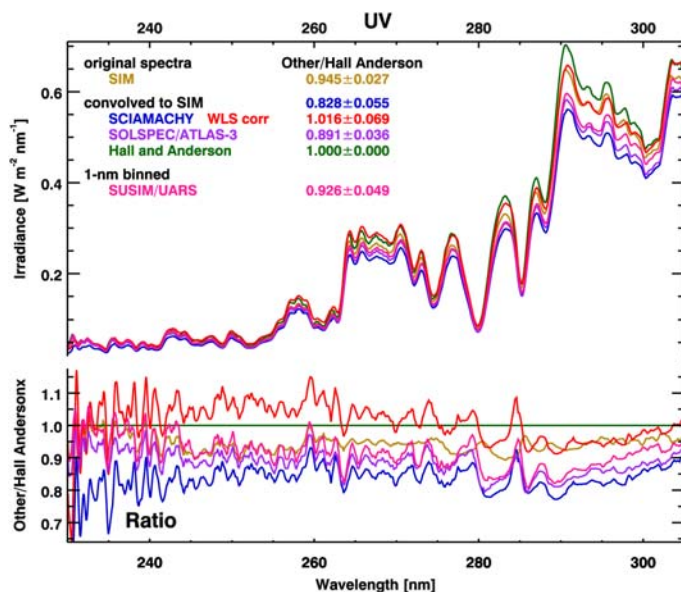

Fig. 3. *Top subpanel*: SIM (tan), SCIAMACHY with (red) and without (blue) WLS corrections, SOLSPEC/ATLAS-3 (purple), Hall & Anderson (green), and SUSIM/UARS (pink) in the 230 nm to 310 nm spectral window. All spectra were convolved to SIM spectral resolution using the SIM instrument functions except for the SUSIM/UARS data, which have been binned to 1 nm. *Bottom subpanel*: ratios of solar data (top) to Hall & Anderson data. Mean ratio of UV spectra to Hall & Anderson data is listed in the upper subpanel.

SOLSPEC/ATLAS-3 convolved to the SIM resolution and 1 nm binned SUSIM/UARS, 1 nm bin being the native spectral resolution in the publicly released of the latter data. The bottom panel shows these spectra integrated into 10 nm bins. The different features and structures are in excellent agreement among all spectra. Overall, there are no significant discrepancies with respect to the wavelength calibration in UV.

Figure 4 shows a plot of absolute irradiances (top subpanel) and ratio (bottom subpanel) of SCIAMACHY (with and without WLS correction) and SIM with respect to Kitt Peak. Overall, the figure suggests differences of less than 3%. A dip of −2% in about 360 nm may be attributed to interference with terrestrial oxygen dimer absorption features, see for example, Greenblatt et al. (1990), that may still be present in Kitt-Peak spectrum used here.

Figures 5 and 6 show convolution of SUSIM and SCIAMACHY spectra to SIM using triangular instrument profiles from UV, vis1, and NIR; and ESR spectrometer channels, respectively. The top subpanels show the original spectra from SUSIM (pink), SCIAMACHY (with and without WLS corrections, red and blue, respectively), and SIM (black). In the UV, SUSIM seems to show high frequency structure, which is enhanced when ESR profile is used. This indicates that SIM ESR becomes noisy towards shorter wavelengths. Both instruments appear to contribute to this structure and have about the same S/N in this spectral region (though SIM has better noise performance from a photodiode detector than a thermal detector with noise floor of about 2 nW Hz$^{1/2}$ with a 40 s integration period).

SCIAMACHY shows an overall bias of less than 5% with respect to SIM across the UV, vis, NIR ranges in each figure. This is valid regardless if WLS correction is applied or not. The largest changes due to the WLS corrections are in the UV region. In the vis region, WLS correction has removed the artefacts near the channel boundary at 600 nm and 800 nm but failed to do
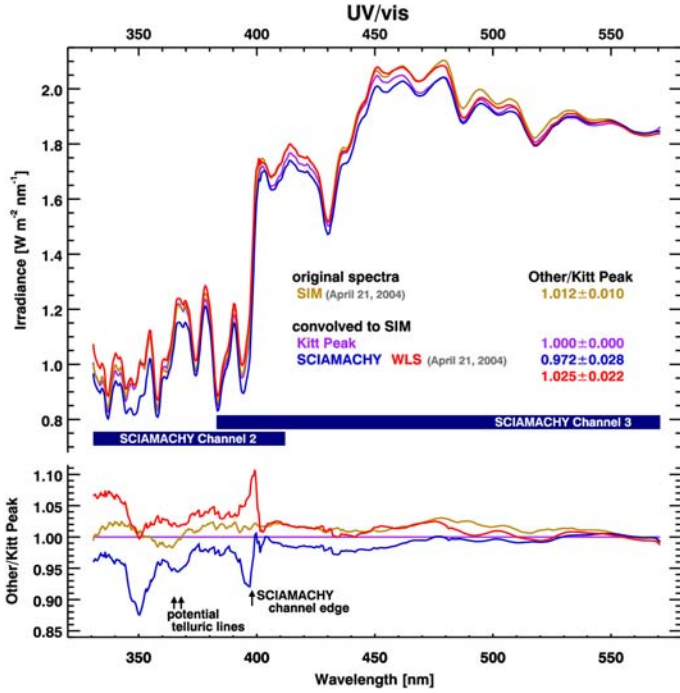
Fig. 4. *Top subpanel*: SCIAMACHY with (red) and without (blue) WLS corrections, SIM (tan), and Kitt Peak (purple) solar data in the 330 to 580 nm spectral range. SCIAMACHY and Kitt Peak data were convolved to the spectral resolution of SIM. *Bottom subpanel*: solar data ratioed to Kitt Peak data. Mean ratio of UV-vis spectra to Kitt Peak data is listed in the upper subpanel.
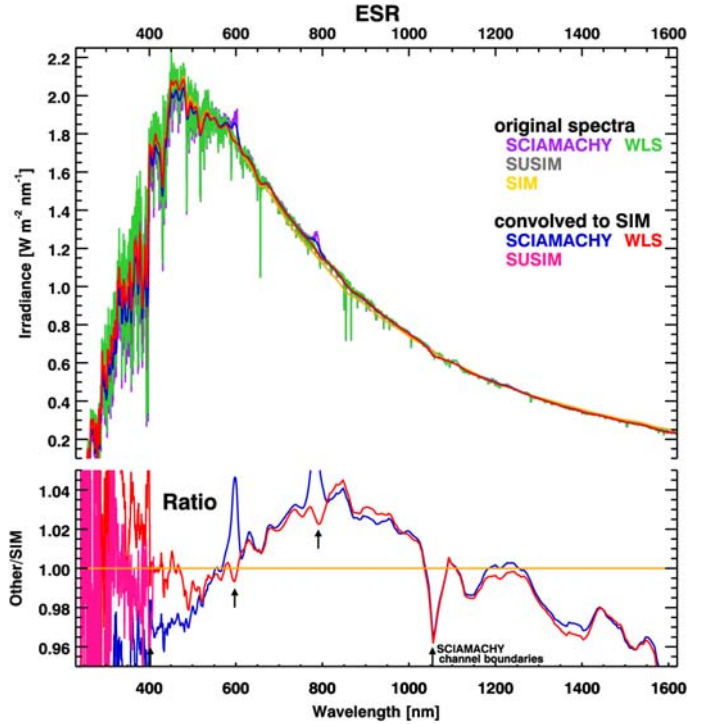

Fig. 5. SCIAMACHY with (red) and without (blue) WLS corrections, SUSIM (pink), SIM (tan) at their native spectral resolution and after convolving to SIM resolutions using instrument functions of SIM's UV, vis1, and NIR channels (*top subpanels*). *Bottom subpanels*: solar ratios of the convolved solar data over SIM. Mean ratio of UV/vis/IR spectra to SIM data is given in Table 2.

the same at 1000 nm. Our results confirm the findings in Skupin et al. (2005a,b) on the UV degradation of the WLS and the overall increase of the WLS output that seems to slightly overcorrect the SCIAMACHY data in the UV.

Fig. 6. SCIAMACHY with (red) and without (blue) WLS corrections, SUSIM (pink) and SIM (tan) at their native spectral resolution and after convolving using SIM's ESR instrument function (*top subpanel*). *Bottom subpanel*: solar ratios with respect to SIM after convolution. Mean ratio of UV-vis-IR spectra to SIM data is given in second and third columns of Table 3.
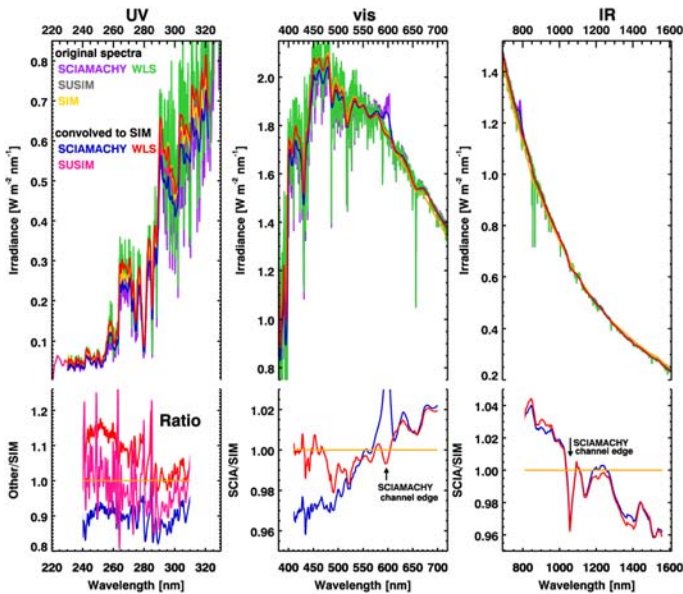
Table 2. Mean ratio of UV/vis/IR Solar Spectra to SIM as shown in bottom subpanels of Fig. 5.

Spectral region	UV	vis	IR
	220–310 nm	410–700 nm	800–1600 nm
Reference spectrum	SIM	SIM	SIM
SUSIM/UARS	0.997 ± 0.081		
SCIAMACHY	0.881 ± 0.059	0.952 ± 0.054	1.003 ± 0.030
SCIAMACHY WLS corr	1.074 ± 0.069	1.027 ± 0.036	0.999 ± 0.029
SIM	1.000 ± 0.000	1.000 ± 0.000	1.000 ± 0.000

In Fig. 7, a comparison to the SOLSPEC/ATLAS-3 composite spectrum is shown. SCIAMACHY shows a bias of 5% and lower except for the channel boundary near 1000 nm. SIM with bias correction agrees to within 4% above 500 nm. At about 750–850 nm, SCIAMACHY shows a small bump. As already pointed out in Pagaran et al. (2009), this bump may be attributed to the aluminum coating of optical elements somewhere along the focal plane. The Wehrli composite shows anomalous dips near 340 nm, 940 nm, 1900 nm, and around 2200–2300 nm, which are most likely telluric absorption features or perhaps due to concatenation process used to join the four datasets as reported by Gueymard (2004).

Convolution of spectra to SIM is appropriate when spectral resolution of spectra are not close to that of SIM. Figures 5–7 shows the extent of SSI in UV regions. Noticeable feature in these figures is the high frequency structure in UV. In this region, the spectral resolution of SIM is about 1.0 nm, which is comparable to SUSIM at 1.1 nm. The comparable spectral resolution
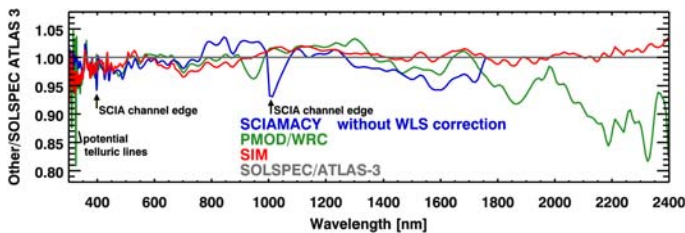
Fig. 7. Ratios of SCIAMACHY (blue), PMOD/WRC (green), and SIM (red) with respect to SOLSPEC/ATLAS-3 (gray) in the visible and NIR. All data have been convolved with SIM's ESR instrument function. Mean ratio of UV-vis-IR spectra to SOLSPEC/ATLAS-3 is given in fourth column of Table 3.

Table 3. Mean ratio of UV/vis/IR Solar Spectra to SIM and SOLSPEC/ATLAS-3 as shown in bottom subpanels of Fig. 6 and in Fig. 7.

Spectral region	UV 220–400 nm	vis-IR 400–1600 nm	UV-vis-IR 300–1700 nm
Reference spectrum	SIM	SIM	SOLSPEC/ ATLAS-3
SUSIM/UARS	0.989 ± 0.060		
SCIAMACHY	0.912 ± 0.040	0.993 ± 0.026	0.995 ± 0.054
SCIAMACHY WLS corr	1.069 ± 0.054	0.999 ± 0.021	
SIM	1.000 ± 0.000	1.000 ± 0.000	0.982 ± 0.040
SOLSPEC/ ATLAS-3			1.000 ± 0.000

coupled with significant uncertainty in wavelength assignment (Woods et al. 1996) and perhaps also due to undersampling and scattered light may have altogether caused this structure. Also optical elements of SUSIM (Floyd 1999) may have degraded after 11 years of operation and exposure to hard UV radiation in space.

3.2. Timeseries comparison of SSI

Here we consider timeseries of measurements from the two instruments and investigate the changes of measured irradiances due to short term solar activity. For this investigation, we selected a period that covers several solar rotations, in particular, from July 3 to August 21, 2004.

In addition to SIM and SCIAMACHY observations, SPM aboard VIRGO/SOHO data are available that covers three small 5–7 nm wide spectral bands in the UV-vis-NIR spectral region. Top subpanels (right to left) of Fig. 8 show VIRGO/SPM Red, Green, and Blue instrument profiles, respectively. Instead of artificially extending Red and Green filters to accommodate more points in the wavelength bands like Unruh et al. (2008) did in their analysis, we interpolate the SSI data to the wavelength bin of the filters. The resulting SSI data are shown in bottom subpanels of Fig. 8. Due to this, we may have the same effect of widening the filters range used in Unruh et al. (2008).

In bottom panels of Fig. 8, it is evident that the high resolution of SCIAMACHY is able to resolve solar absorption features. Among them, Ca II doublet at 393.4 and 396.8 nm in UV (left); bunch of lines: e.g., He I at 492 and 502 nm, Ba II at 493 nm and Fe I at 495.8 nm in vis (middle); two of the Ca II triplet at 854.2 and 866.2 nm (849.8 nm not shown) in NIR (right).

Using a five-point Newton-Cotes integration, we integrated the area under the curves covered by SIM and SCIAMACHY
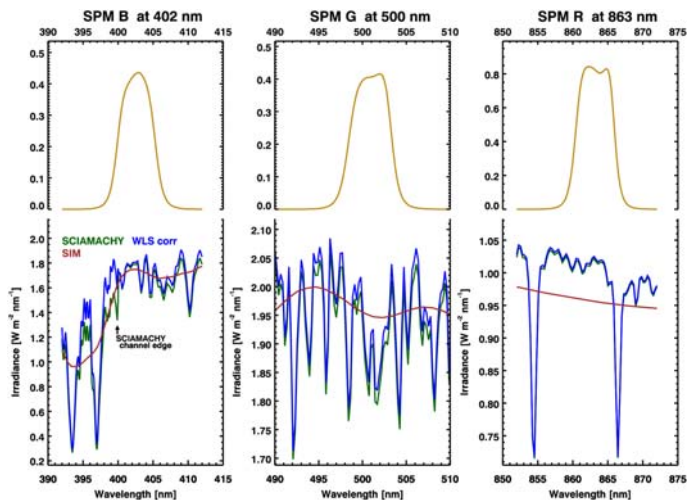

Fig. 8. *Top subpanels* show Red (*right*), Green (*center*), and Blue (*left*) bandpass filters of SPM/VIRGO. *Bottom subpanels* show spectra from SIM (brown), uncorrected (green) and WLS corrected (blue) SCIAMACHY at their native spectral resolution.

SSI data over the wavelength range of the SPM filters. Taking fractional difference to July 14, 2004 in all SSI data, the resulting time series are shown in Fig. 9. In addition, TSI data from PMOD/WRC (daily) and TIM/SORCE (every six hours) are also plotted. We confirm the overall good agreement found by Unruh et al. (2008) between VIRGO/SOHO and SIM/SORCE. In all channels and in the narrow time interval considered, we did not observe any further enhancements due to brightening of faculae near the limb that was seen by Unruh et al. (2008) during June 20–24, 2004. Comparison between VIRGO/SOHO and SCIAMACHY/ENVISAT (both uncorrected and WLS corrected) shows good agreement in Red filter especially from 3 to 29 of July 2004. In Green and Blue filters, SCIAMACHY reproduces the pattern of rise and fall due to solar activity but a small bias on the order of 0.1% and a small trend in the SCIAMACHY data is evident.

Comparison of SSI data to TSI from PMOD/WRC and TIM/SORCE, shows that in general behavior of TSI is similar in all three filters. However, a closer look at the July 22, 2004 sunspot depression shows that sunspot minima of SSI data are deeper in Blue (about a factor of 2) than in Green (about a factor of 1.5) if compared to the sunspot minima of TSI data. In Red, there is a reversed behaviour where sunspot minima of TSI data are deeper by about 10% than SSI data.

3.3. Comparison of integrated SSI

In Harder et al. (2005c) and Rottman (2006), for example, time series of SIM irradiance at selected wavelength points (430 nm, 656 nm, 857 nm, and 1000 nm) were compared to TSI. Unruh et al. (2008) integrated SIM from 220 to 1660 nm and compared to TSI and to integrated SSI from the SATIRE model. Meanwhile, in Harder et al. (2008), integrated SSI from SIM have been computed at various wavelength ranges; but they were not compared to TSI.

We integrate SSI data measured by the three instruments on April 21, 2004 using following wavelength intervals: 10 nm, 50 nm, and 100 nm, broad bands in the UV (240–310 nm), vis (400–700 nm), and NIR (700–1600 nm), respectively. The integrated SSI areas are provided in Tables 4–6. Overall, uncorrected SCIAMACHY (WLS-corrected) tends to show low
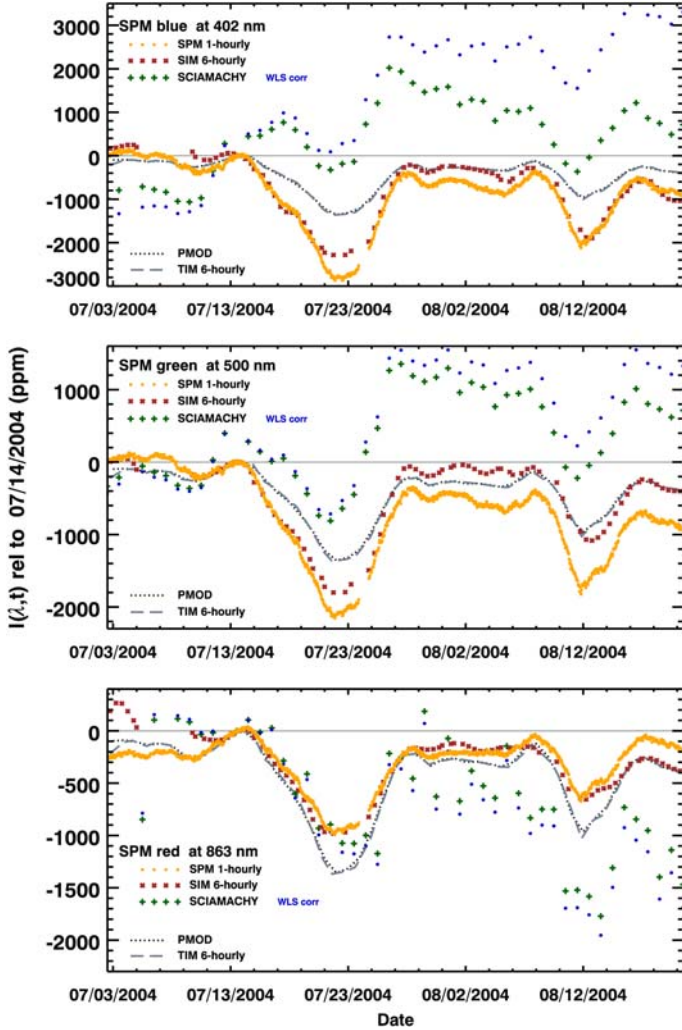
Fig. 9. SSI time series comparison. Shown are hourly SPM data (orange dots), 6-hourly SIM (brown ×), daily SCIAMACHY (green +), and WLS corrected SCIAMACHY spectra (blue dots) at Red (*bottom panel*), Green (*middle panel*), and Blue (*top panel*) filters of SPM. All data are shown with respect to data from July 14, 2004. Daily spectra from SIM and SCIAMACHY are convolved to SPM RGB bandpass filters.

bias (high bias) compared to SUSIM in UV and SIM in UV-vis-NIR. In general, areas from SIM are intermediate between WLS-corrected and uncorrected SCIAMACHY in UV-vis-NIR, and SUSIM in UV indicating again that WLS correction are too strong due to starting optical degradation of WLS. In 2004, the WLS correction still generally improves the present comparison particularly in those bands that include SCIAMACHY channel boundaries as indicated by bold typeface entries in Tables 4–6.

By considering the same time period in July and August 2004 as above, we integrate SSI at selected spectral regions, namely UV, vis, NIR, and entire UV/vis-NIR regions corresponding to 240–400 nm, 400–700 nm, 700–1600 nm, and 240–1600 nm, respectively. The vis interval coincides to one of the intervals considered by Harder et al. (2008). The UV/vis-NIR interval almost coincides with the wavelength coverage considered by Unruh et al. (2008), which was from 220–1660 nm. Our starting wavelength range at 240 nm is restricted by the SCIAMACHY wavelength range. The time period, on the other hand, covers a subset used by Unruh et al. (2008), i.e., last month of their time period with 21 additional days in August 2004.

Table 4. Integrated solar irradiance in units of W m^{-2} at 10-nm wavelength intervals in UV spectral region (240–310 nm).

Instrument	Integrated UV SSI [W m^{-2}]			
	SUSIM	SCIAMACHY		SIM
λ-interval [nm]		uncorr	WLS-corr	
240–250*	0.56	0.48	**0.61**	0.54
250–260	0.80	0.74	0.92	0.80
260–270	1.93	1.81	2.21	2.01
270–280	1.71	1.82	2.17	1.99
280–290	2.81	2.64	3.11	3.02
290–300	5.21	4.89	5.65	5.61
300–310	5.69	5.34	5.99	5.86
total area [W m^{-2}]	18.71	17.72	20.67	19.84

Notes. We use solar spectra measured by the three instruments on April 21, 2004. Wavelength interval with * denotes interval containing SCIAMACHY channel boundaries.

Table 5. Same as Table 4 except at 50-nm wavelength intervals in vis spectral region (400–700 nm).

Instrument	Integrated vis SSI [W m^{-2}]		
	SCIAMACHY		SIM
λ-interval [nm]	uncorr	WLS-corr	
400–450*	85.45	**88.01**	88.14
450–500	98.84	100.98	101.66
500–550	93.72	94.23	95.10
550–600	92.51	91.15	91.43
600–650*	84.19	**83.66**	82.95
650–700	75.68	75.58	74.45
total area [W m^{-2}]	530.38	533.61	533.71

Table 6. Same as Tables 4, 5 except at 100-nm wavelength intervals in NIR spectral region (700–1600 nm).

Instrument	Integrated NIR SSI [W m^{-2}]		
	SCIAMACHY		SIM
λ-interval [nm]	uncorr	WLS-corr	
700–800*	130.18	**128.80**	125.50
800–900	103.11	103.33	99.82
900–1000	83.45	83.70	81.63
1000–1100	66.72	66.62	66.88
1100–1200	54.49	54.37	54.82
1200–1300	45.68	45.50	45.76
1300–1400	37.79	37.65	38.78
1400–1500	31.84	31.82	32.73
1500–1600	26.57	26.51	27.78
total area [W m^{-2}]	579.82	578.30	573.71

Figure 10 shows integrated SSI time series at these selected spectral regions as changes with respect to July 14, 2004, along with variations in TSI. The overall variability is in agreement with integrated SSI from SIM over the same wavelength range. In the 240–1600 nm band (bottom panel) TSI time series closely agree with integrated SSI. This suggests that spectral regions shorter than 240 nm and longer than 1600 nm contribute very little to TSI. A closer look at the solar rotation minima, integrated SSI in the visible range are deeper than TSI, while in the NIR they appear shallower and over the entire UV/vis-NIR (almost agree) with TSI. Depending on wavelength contributions from both sunspot darkening and faculae brightening compete with
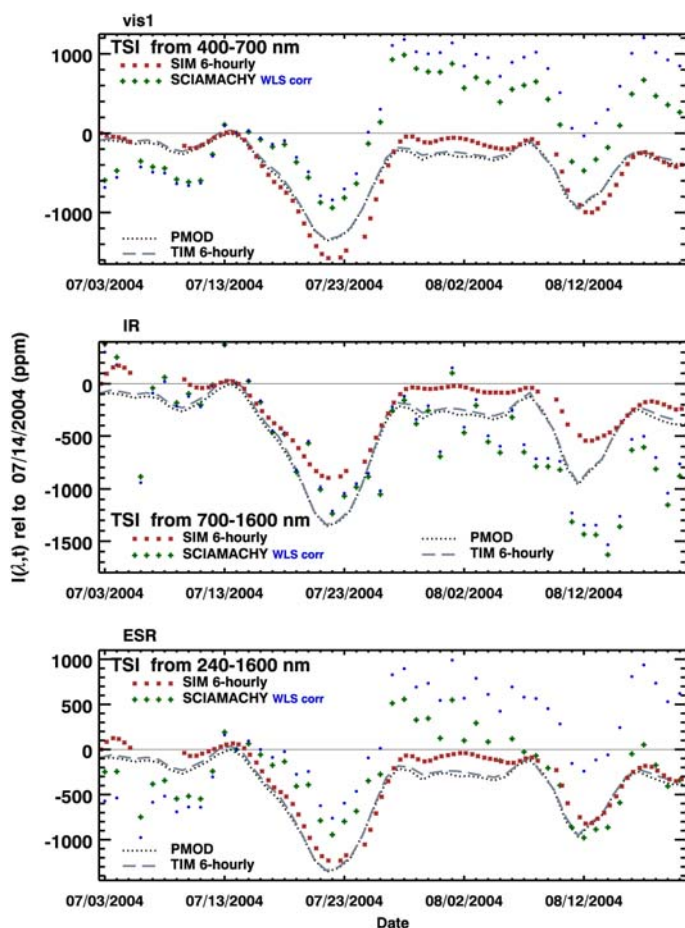
Fig. 10. Integrated SSI time series comparison. Shown in this figure *from top to bottom* panels are time series of SSI integrated over vis (400–700 nm), NIR (700–1600 nm), and entire UV/vis-NIR (240–1600 nm) spectral regions, respectively.

different magnitudes. Integrated SSI time series seem to appear slightly ahead in time relative to TSI. This is obviously the case in the visible (top panel) and NIR (middle panel) spectral range. This can be attributed to active region transiting the solar disk, i.e., sunspot moving towards the disk-center (vis-IR depleting) and faculae approaching the limb (UV enhancing) during descending and ascending phases, respectively. The active region and their spectrally dependent enhancing or depleting effects compensate each other when integrating over 240 to 1600 nm. Finally, the TSI time series appear to have slightly more negative trends than the integrated SSI time series in all spectral regions (vis, IR, and UV-vis-IR). Whether this is in agreement with results in Fröhlich (2009) that during solar cycle 23 TSI has generally a stronger downward trend than SSI in the visible and IR remains an open issue.

4. Discussion and conclusion

Measurements in the spectral regions UV, vis, NIR, and integrated over UV-vis-NIR range from SCIAMACHY and SIM spectrometers are compared to selected reference spectra from ground-based measurements (Kitt Peak or new Kurucz), high-altitude balloons (Hall and Anderson, Neckel and Labs, and Wehrli composite); and from space-borne measurements (SOLSPEC/ATLAS-3 composites, and SUSIM/UARS).

Figures 3 and 7 show comparisons of SCIAMACHY and SIM with balloon data from Hall & Anderson, Kitt-Peak FTS data, and Wehrli composite. Overall, the agreement to these reference data is quite good and generally within 4% across the UV and visible. These reference spectra were taken inside the Earth's atmosphere so telluric contributions limit the range to 300–900 nm. They and their composites (e.g., Wehrli composite) may still contain atmospheric interferences such as strong absorption bands by oxygen dimer, ozone, water vapor, carbon dioxide and other gases that may lead to larger differences but still remain within 4% of space SSI. There is also an issue on how well the conversion from original disk-center radiance, where most of these reference spectra are obtained, to disk-average irradiance, as usually measured from space, is achieved. This conversion is performed by applying some empirical spectral corrections such as spatially inhomogenous solar surface with limb-darkening effects (Gueymard 2004, 2006).

The intercomparison between SIM and SCIAMACHY as shown in Figs. 5 and 6 shows that SCIAMACHY underestimates SIM and SUSIM by up to 10% in the UV below 300 nm. The WLS correction of the SCIAMACHY data on the other hand leads to an overestimation which shows that the optical degradation of the WLS leads to a too strong SSI degradation correction. In the visible-NIR region SCIAMACHY and SIM agree to better than 4%. The WLS correction leads to a better agreement near 600 m, at the end of SCIAMACHY channel 4 and begin of channel 5. Near the boundary of Channels 5 and 6 near 1000 nm no improvement is achieved by applying the WLS correction. Similar results are obtained in the comparisons to the SOLSPEC/ATLAS-3 composite as shown in Fig. 7. The bias corrected SIM spectra show very good agreement to within 2% with the SOLSPEC/ATLAS-3 composite over the entire wavelength region up to 2400 nm. Up to 1700 nm SCIAMACHY agrees with the SOLSPEC/ATLAS-3 composite to within 3%.

Integrated SSI at distinct wavelength intervals in UV (over 10 nm), vis (over 50 nm), and NIR (over 100 nm) from the two spectrometers are also compared (Tables 4–6). For wavelength intervals covered by two adjacent channels in SCIAMACHY, the WLS corrected SCIAMACHY data agree better with SUSIM and SIM than the uncorrected data. For longer periods covering few 27-day solar rotations in 2004 we also compared SSI time series from the two spectrometers to RGB filters in SPM VIRGO (see Fig. 9) and to TSI time series from PMOD/WRC composite and from TIM/SORCE (see Figs. 9 and 10). Both SCIAMACHY and SIM track each other well over several solar rotations. In the visible and near IR the SSI changes are in sync with the TSI. This is expected since vis-IR is dominated by contributions from sunspots that darkens in contrast to brightening of faculae. Agreement between SIM and SPM/VIRGO is very good, while agreement with SCIAMACHY is slightly worse. In the visible the SSI solar rotational minima are deeper in the visible compared to TSI and shallower in the NIR. From Fig. 10 it is also evident that the SSI time series slightly lags the TSI time series in the visible and NIR due to sunspot moving towards the disk-center (vis-IR depleting) and faculae approaching the limb (UV enhancing) during descending and ascending phases in the solar rotation cycle.

With SCIAMACHY and SIM now operating for several years, our knowledge in SSI variability is beginning to be reliably quantified in the vis-IR. Intercomparisons as presented are important to assess the quality of continuity and homogeneity of SSI datasets from different spectrometers.

Appendix A: Description of instruments

In this appendix, we provide additional information on the two spectrometers. We provide simplified block diagram showing the optical path involved in measuring solar light and in calibrating the optical elements. Also, a summary of the instrumental parameters is given for each spectrometer.

A.1. Instrumental parameters and optical paths

Figure A.1 shows schematically the optical paths of the SCIAMACHY and SIM spectrometers, respectively. Instrumental parameters are summarized in Tables A.1 and A.2.

A.2. In-flight calibration mechanisms

SCIAMACHY's in-flight calibration. For in-flight calibration, SCIAMACHY has two internal light sources. These sources are a PtCrNe-hollow cathode lamp as spectral light source (SLS), and a 5 Watt quartz-tungsten-halogen lamp as a white light source (WLS), for wavelength and etalon calibration, respectively. Both lamps can be observed only with the ESM mirror or ESM diffuser in the nadir optical path (cf. Fig. A.2).

Due to lack of SLS lines in channels 7 and 8 (>1700 nm), only Channels 1 to 6 are covered by the in-flight wavelength calibration. As shown in Bovensmann et al. (2002), SCIAMACHY's wavelength calibration is stable to within 0.02 nm.

In-flight WLS radiometric calibration is used to correct pixel- (e.g., pixel-to-pixel gain) and wavelength-dependent (e.g., etalon) effects including temperature dependent quantum efficiency of detectors and throughput changes of optical bench module components. Like the assumption made in SLS, small (first order, i.e., linear) changes between on-ground and in-flight are presumed; these changes are given by the ratio between dark signal corrected on-ground and in-flight WLS measurements. The WLS lamps are not radiometrically calibrated, however, changes between on-ground and in-flight WLS measurements can be compared to solar irradiance changes with respect to the start of the mission to track optical degradation changes with time. However, WLS also suffers from optical degradation that is accelerating more strongly than the ESM diffuser solar irradiances and can, therefore, not be used for degradation monitoring beyond year 2004.

Figure A.3 shows an example for a wavelength dependent degradation correction based upon WLS ratios. It is assumed that
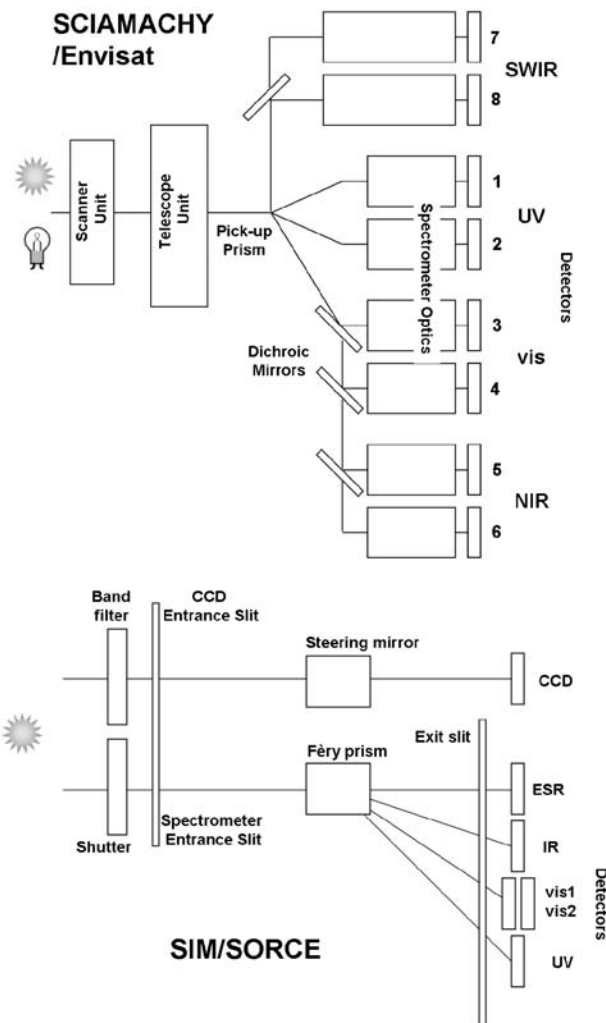
Fig. A.1. Simplified block diagrams of SCIAMACHY (*top*) and SIM (*bottom*) spectrometers. External (internal) light source such as the sun (calibration lamps) are indicated on the left-hand-side. Detectors, i.e., photodiodes, which convert light to electronic signals, are indicated in the right-hand-side. For summary of SCIAMACHY and SIM instrumental parameters, see Tables A.1 and A.2, respectively.
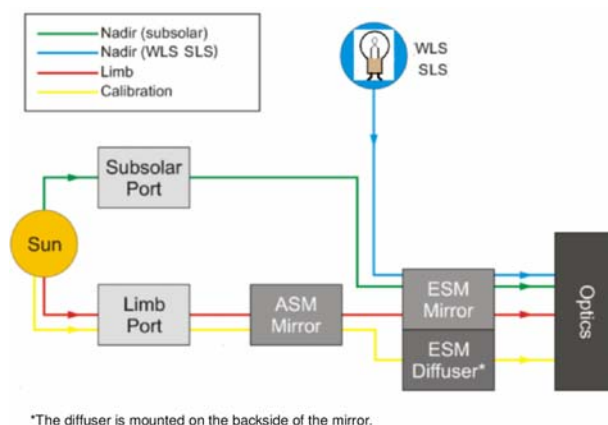

Fig. A.2. Schematic view of SCIAMACHY monitoring light paths. SCIAMACHY has three light paths used for scientific measurements, namely: the calibration (ASM mirror and ESM diffuser), limb (ASM mirror and ESM mirror), and nadir (ESM mirror). Shown also are internal light sources, namely: white light (WLS) and spectral line (SLS) sources for in-flight irradiance and wavelength calibration purposes, respectively (cf. Sect. A.2). Source: Modified Figs. 5, 6 of Gottwald et al. (2006).

Table A.1. Summary of SCIAMACHY instrumental parameters.

Instrument	SCIAMACHY[a]
spectrometer type	multi-channel grating
Platform	ENVISAT[b]
Agency	ESA
Launch date	March 1, 2002
Operation	2002-present
IFOV	$0.045° \times 1.8°$
Wavelength range	(214) 240–1750 nm, 1940–2040 and 2265–2380 nm
Spectral resolution	0.2—1.48 nm
Solid state devices	Si (Channels 1–5), InGaAs (Channels 6–8)
Mass	198 kg
Power	122 W
Data rate	400–1900 kbps (mode-dependent)
Special modes	nadir, limb, and solar-occultation
Preflight calibration	NIST cryogenic radiometer
Inflight calibration	white light (WLS), and spectral line (SLS) sources
Heritage	GOME/ERS-2
References	Bovensmann et al. (1999); Gottwald et al. (2006)

Notes. [a] **SC**anning **I**maging **A**bsorption Spectro**M**eter for **A**tmospheric **CH**artograph**Y**. [b] **Envi**ronmental **Sat**ellite.

Table A.2. Summary of SIM instrumental parameters.

Instrument	SIM[a]
spectrometer type	dual Fèry prism
Platform	SORCE[b]
Agency	NASA
Launch date	January 25, 2003
Operation	2003-present
IFOV	$1.7° \times 2.5°$
Wavelength range	300–2400 nm
Spectral resolution	0.25–33 nm
Solid state devices	ESR, InGaAs
Mass	22 kg
Power	25 W
Data rate	0.65 Mbps
Special modes	ESR, photodiode fast scan, fixed wavelength, NIR scan
Preflight calibration	Component unit level test + NIST cryogenic radiometer
Inflight calibration	Prism transmission cal + redundant channel comparison
Heritage	new but developed to replace and extend SOLSTICE/UARS
References	Harder et al. (2000, 2005a,b)

Notes. [a] **S**pectral **I**rradiance **M**onitor. [b] **SO**lar **R**adiation and **C**limate **E**xperiment.

the change with respect to preflight conditions can be expressed by the ratios of two Planck curves as follows

$$r_{\text{WLS}} = a \frac{B(\lambda, T_{\text{preflight}} + \Delta T)}{B(\lambda, T_{\text{preflight}})}, \tag{A.1}$$

where a and ΔT are fitting parameters. In space a change in lamp temperature (ΔT) from preflight conditions has to be accounted for. The fitting parameters are derived from fits to part of the WLS ratios marked red (spectral channels 4 to 6) in Fig. A.3, where optical degradation is smallest. The difference between the fitted WLS ratio to the observed one yields the SSI degradation curve.

SIM's in-flight calibration. SIM employs a two spectrometer comparison technique to track long-term degradation, a detailed description of this degradation method can be found in the auxillary material to Harder et al. (2009). Changes in prism transmission are initiated by long term exposure of prism from ionizing radiation, where either the radiation degrades the prism glass or a thin film of organic material accumulates on the surface.

SIM maintains its wavelength scale through a precision prism drive that has a wavelength error of about 150 ppm depending on wavelength. Through a separate optical path, the wavelength precision is achieved by implementing a closed loop wavelength drive system: (1) a voice coil actuated turntable to rotate the prism and (2) a charged coupled device (CCD) linear array in the spectrometer's focal plane to detect the prism rotation angle. The basic principle is based on the following. As the prism rotates, the image spot moves along the length of the CCD giving the angle of rotation and therefore the wavelength of light going through each of the detector's exit slits.
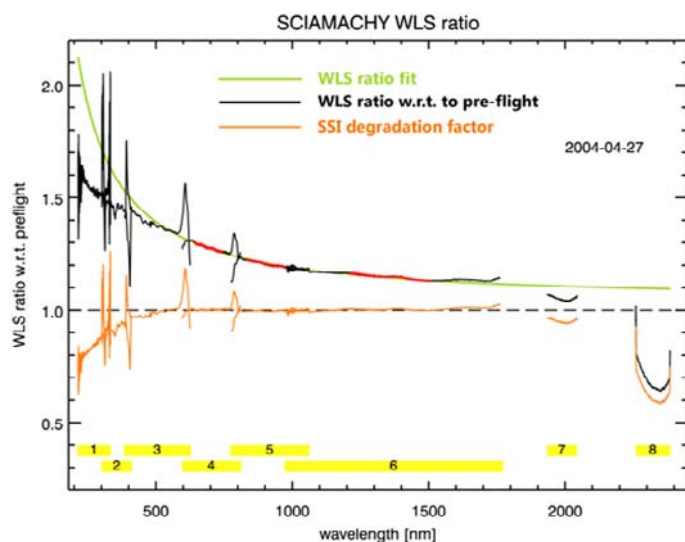
Fig. A.3. SCIAMACHY WLS ratios with respect to preflight conditions. Black curve shows the ratio of WLS spectra measured in April 27, 2004, with respect to a spectrum measured before launch. A ratio of two Planck curves with different temperatures accounting for changes in lamp temperatures in space is fitted in Channel 4 to 6 (see red marked lines) to obtain a theoretical WLS ratio (green curve). The difference of the fitted WLS ratio to the observed one yields the SSI degradation factor for April 2004 (orange line).

References

Anderson, G. P., & Hall, L. A. 1989, J. Geophys. Res., 94, 6435
Arnold, N. 2002, Roy. Soc. of London Proc. A, 360, 2787
Berdyugina, S. V. 2005, Liv. Rev. Sol. Phys., 2
Bovensmann, H., Ahlers, B., Buchwitz, M., et al. 2002, in Proc. of the Envisat calibration review, SP-520, ESA Publications Division, ed. H., Sawaya-Lacoste, 520, 1
Bovensmann, H., Burrows, J. P., Buchwitz, M., et al. 1999, J. Atmos. Sci., 56, 127
Brueckner, G. E., Edlow, K. L., Floyd, L. E., Lean, J. L., & Vanhoosier, M. E. 1993, J. Geophys. Res., 98, 10695
Brueckner, G. E., Floyd, L. E., Lund, P. A., Prinz, D. K., & Vanhoosier, M. E. 1995, Metrologia, 32, 661
Burrows, J. P., Weber, M., Buchwitz, M., et al. 1999, J. Atmos. Sci., 56, 151
de Wit, T. D., & Watermann, J. 2010, Comptes Rendus Geosciences, 342, 259
Dobber, M., Voors, R., Dirksen, R., Kleipool, Q., & Levelt, P. 2008, Sol. Phys., 249, 281
Domingo, V., Ermolli, I., Fox, P., et al. 2009, Space Sci. Rev., 145, 337
Fligge, M., Solanki, S. K., Unruh, Y. C., Fröhlich, C., & Wehrli, C. 1998, A&A, 335, 709
Fligge, M., Solanki, S. K., & Unruh, Y. C. 2000, A&A, 353, 380
Floyd, L. 1999, Adv. Space Res., 23, 1459
Floyd, L. E., Cook, J. W., Herring, L. C., & Crane, P. C. 2003, Adv. Space Res., 31, 2111
Fontenla, J., & Harder, G. 2005, Mem. Soc. Astron. Italiana, 76, 826
Fontenla, J. M., Harder, J., Rottman, G., et al. 2004, ApJ, 605, L85
Fröhlich, C. 2003, Metrologia, 40, 60
Fröhlich, C. 2009, A&A, 501, L27
Fröhlich, C., & Lean, J. 1998, in New Eyes to See Inside the Sun and Stars, ed. F.-L. Deubner, J. Christensen-Dalsgaard, & D. Kurtz (Dordrecht: Kluwer Academic Publishers), IAU Symp. 185, 89
Fröhlich, C., & Lean, J. 2004, A&ARv, 12, 273
Fröhlich, C., Romero, J., Roth, H., et al. 1995, Sol. Phys., 162, 101
Gottwald, M., Bovensmann, H., Lichtenberg, G., et al. 2006, SCIAMACHY, monitoring the changing Earth's atmosphere, DLR Institut für Methodik der Fernerkundung (IMF), Oberpfaffenhofen
Gray, L., Beer, J., Geller, M., et al. 2010, Rev. Geophys., 48, RG4001
Greenblatt, G. D., Orlando, J. J., Burkholder, J. B., & Ravishankara, A. R. 1990, J. Geophys. Res., 95, 18577
Gueymard, C. 2004, Solar Energy, 76, 423
Gueymard, C. A. 2006, Adv. Space Res., 37, 323

Gurlit, W., Bösch, H., Bovensmann, H., et al. 2005, Atmos. Chem. Phys., 5, 1879
Haigh, J. D. 2003, Roy. Soc. of London Proc. A, 361, 95
Haigh, J. D. 2007, Liv. Rev. Sol. Phys., 4, http://www.livingreviews.org/lrsp-2007-2
Hall, J. A. 2008, Liv. Rev. Sol. Phys., 5
Hall, L. A., & Anderson, G. P. 1984, J. Geophys. Res., 89, 7322
Hall, L. A., & Anderson, G. P. 1991, J. Geophys. Res., 96, 12927
Harder, J. W., Lawrence, G. M., Rottman, G. J., & Woods, T. N. 2000, in Proc. SPIE, ed. W. L. Barnes, 4135, 204
Harder, J. W., Lawrence, G., Fontenla, J., Rottman, G., & Woods, T. 2005a, Sol. Phys., 230, 141
Harder, J. W., Fontenla, J., Lawrence, G., Woods, T., & Rottman, G. 2005b, Sol. Phys., 230, 169
Harder, J. W., Fontenla, J., White, O., Rottman, G., & Woods, T. 2005c, Mem. Soc. Astron. Italiana, 76, 735
Harder, J. W., Fontenla, J., Pilewskie, P., Richard, E., & Woods, T. 2008, AGU Fall Meeting Abstracts, A1630
Harder, J. W., Fontenla, J. M., Pilewskie, P., Richard, E. C., & Woods, T. N. 2009, Geophys. Res. Lett., 36, L07801
Harder, J. W., Thuillier, G., Richard, E. C., et al. 2010, Sol. Phys., 263, 3
Hoyt, D. V., & Schatten, K. H. 1997, The Role of the Sun in Climate Change (Oxford: Oxford University Press)
Hudson, H. S. 1988, ARA&A, 26, 473
Intergovernmental Panel on Climate Change (IPCC) Report 2001, Climate Change 2001: The Scientific Basis (Cambridge University Press)
Kopp, G., Lawrence, G., & Rottman, G. 2005, Sol. Phys., 230, 129
Krivova, N. A., Solanki, S. K., & Floyd, L. 2006, A&A, 452, 631
Krivova, N. A., Solanki, S. K., & Unruh, Y. 2011, J. Atmos. Sol.-Terr. Phys., 73, 223
Krivova, N. A., Solanki, S. K., Wenzler, T., & Podlipnik, B. 2009, J. Geophys. Res., 114, D00I04
Kurucz, H. L. 1995, in Laboratory and astronomical high resolution spectra, ed. A. J. Sauval, R. Blomme, & N. Grevesse, ASP Conf. Ser., 81, 17
Labs, D., & Neckel, H. 1968, Z. Astrophys., 69, 1
Lean, J. 1987, J. Geophys. Res., 92, 839
Lean, J. 1997, ARA&A, 35, 33
Lean, J., & Rind, D. 2001, Science, 292, 234
Lean, J., Rottman, G., Harder, J., & Kopp, G. 2005, Sol. Phys., 230, 27
Lean, J. L., Rottman, G. J., Kyle, H. L., et al. 1997, J. Geophys. Res., 102, 29939
Nandy, D., & Martens, P. C. H. 2007, Adv. Space Res., 40, 891
Neckel, H., & Labs, D. 1981, Sol. Phys., 74, 231
Neckel, H., & Labs, D. 1984, Sol. Phys., 90, 205
Pagaran, J., Weber, M., & Burrows, J. 2009, ApJ, 700, 1884
Piters, A. J. M., Bramstedt, K., Lambert, J., & Kirchhoff, B. 2006, Atmos. Chem. Phys., 6, 127
Priest, E. R. 2009, in Proc. of the 15th Cambridge Workshop on Cool Stars, Stellar Systems and the Sun, ed. E. Stempels, AIP Conf. Proc., 1094, 3
Rind, D., Lean, J., Lerner, J., Lonergan, P., & Leboissitier, A. 2008, J. Geophys. Res. (Atmospheres), 113, D24103
Rottman, G. 2005, Sol. Phys., 230, 7
Rottman, G. 2006, Space Sci. Rev., 125, 39
Rottman, G., Floyd, L., & Viereck, R. 2004, Geophys. Mono., 41, 111
Rottman, G. J., & Woods, T. N. 1994, in Proc. SPIE
Rottman, G. J., Woods, T. N., & Sparn, T. P. 1993, J. Geophys. Res., 98, 10667
Skupin, J., Noël, S., Wuttke, M. W., et al. 2005a, Adv. Space Res., 35, 370
Skupin, J., Weber, M., Noël, S., Bovensmann, H., & Burrows, J. P. 2005b, Mem. Soc. Astron. Italiana, 76, 1038
Thuillier, G., Floyd, L., Woods, T. N., et al. 2004, in Solar Variability and its Effects on Climate, Geophysical Monograph 141, ed. J. M. Pap, P. Fox, C. Fröhlich, H. S. Hudson, J. Kuhn, J. McCormack, G. North, W. Sprigg, & S. T. Wu, 141, 171
Tobiska, W. K., & Bouwer, S. D. 2006, Adv. Space Res., 37, 347
Tobiska, W. K., Woods, T., Eparvier, F., et al. 2000, J. Atmos. Sol.-Terr. Phys., 62, 1233
Unruh, Y. C., Krivova, N. A., Solanki, S. K., Harder, J. W., & Kopp, G. 2008, A&A, 486, 311
Weber, M., Burrows, J. P., & Cebula, R. P. 1998, Sol. Phys., 177, 63
Wehrli, C. 1985, Extraterrestrial Solar Spectrum, Tech. Rep., Physikalisch-Meteorologisches Observatorium, World Radiation Center (PMO/WRC), Publication No. 615
Wehrli, C., & Fröhlich, C. 1991, Metrologia, 28, 285
Woods, T. N., & Rottman, G. J. 2002, Solar Ultraviolet Variability Over Time Periods of Aeronomic Interest (AGU, Washington, DC), 221
Woods, T. N., Prinz, D. K., Rottman, G. J., et al. 1996, J. Geophys. Res., 101, 9541